GEOLOGY

A revised position for the primary strand of the Pleistocene-Holocene San Andreas fault in southern California

Kimberly Blisniuk[1]*, Katherine Scharer[2], Warren D. Sharp[3], Roland Burgmann[4], Colin Amos[5], Michael Rymer[6]

The San Andreas fault has the highest calculated time-dependent probability for large-magnitude earthquakes in southern California. However, where the fault is multistranded east of the Los Angeles metropolitan area, it has been uncertain which strand has the fastest slip rate and, therefore, which has the highest probability of a destructive earthquake. Reconstruction of offset Pleistocene-Holocene landforms dated using the uranium-thorium soil carbonate and beryllium-10 surface exposure techniques indicates slip rates of 24.1 ± 3 millimeter per year for the San Andreas fault, with 21.6 ± 2 and 2.5 ± 1 millimeters per year for the Mission Creek and Banning strands, respectively. These data establish the Mission Creek strand as the primary fault bounding the Pacific and North American plates at this latitude and imply that 6 to 9 meters of elastic strain has accumulated along the fault since the most recent surface-rupturing earthquake, highlighting the potential for large earthquakes along this strand.

INTRODUCTION

Landforms offset along faults by surface-rupturing earthquakes preserve a cumulative record of fault motion over time. When combined with their ages of formation, these offset landforms may be used to calculate average long-term fault-slip rates. Slip rate data, especially over multiple time intervals, are fundamental to understanding the kinematic partitioning of deformation along an evolving plate boundary. These slip rate data are also important when evaluating earthquake hazard because in most long-term probabilistic seismic hazard models, the faster a fault slips, the greater the likelihood of a future earthquake [e.g., (1, 2)].

The faults of the southern San Andreas fault system, inclusive of the San Andreas fault (SAF), San Jacinto fault, and Elsinore fault (Fig. 1A), all accommodate Pacific–North American (PA-NA) plate motion and all pose seismic hazard (1). Of these, the SAF poses the greatest hazard potential because the southernmost section has not ruptured since ca. 1726 CE (Fig. 1A) (3), and geodetic data suggest that the fault accumulates interseismic strain of up to 25 mm/year, roughly half of the motion across the PA-NA plate boundary [(4) and references therein]. However, the SAF is multistranded along this section so it is uncertain which strand of the SAF carries the most slip and poses the greatest rupture likelihood [e.g., (5, 6)]. Furthermore, obtaining geologic slip rates for some strands of the fault has proven challenging, while geodetic slip rate models have limited resolution in places where faults are closely spaced or multistranded, as the SAF is in southern California.

In the Coachella Valley in southern California near the Indio Hills, at the Biskra Palms site, the SAF is estimated to slip at a rate of ~12 to 22 mm/year (14 to 17 mm/year, preferred) (Fig. 1A) (7). Northwest

of this location, the SAF bifurcates into the Mission Creek and Banning strands (Fig. 1A). Farther northwest, the SAF further partitions and encompasses the Mission Creek, Banning, and Garnet Hill strands and San Gorgonio Pass fault zone (Fig. 1A). Here, the relative proportion of plate boundary deformation accommodated by each strand of the SAF remains unresolved (7–11), despite the distinct implications that slip rates would have on earthquake rupture forecasts and understanding the tectonic configuration of this complex region. Several studies suggest that the majority of plate boundary deformation is localized along the Banning and Garnet Hill strands and the San Gorgonio Pass fault zone (Fig. 1B) because kinematic models for the region infer that the Mission Creek strand and its northwest continuation as the Mill Creek strand is inactive [(8–11) and references therein]. The Banning and Garnet Hill strands and San Gorgonio Pass fault zone are assumed by current hazard models (1) to take up most of the lateral strain at this latitude and, therefore, are considered most likely to rupture in a future SAF earthquake (12).

Many kinematic models indicate that as the SAF bifurcates northwestward into the Mission Creek and Banning strands at Biskra Palms, slip on the Mission Creek strand diminishes to the northwest. For example, slip rates on the Mission Creek strand are thought to decrease from values of 14 to 17 mm/year at Biskra Palms (7) to ~2 to 6 mm/year (13) at the Thousand Palms site located in the Indio Hills and 0 to 3 mm/year near the San Bernardino Mountains ~30 km to the northwest (Fig. 1A) [(1) and references therein]. Near Thousand Palms, the majority of SAF slip has been inferred to occur along the Banning strand [(7–11) and references therein]. The postulated reduction in slip rate and, therefore, diminished rupture likelihood on the Mission Creek strand has been explained by a model of regional fault reorganization that attributes transfer of slip off the Mission Creek strand to a change in fault geometry as the SAF evolves to a restraining bend near the southern Little San Bernardino Mountains (9–11). This transfer of plate boundary deformation off of the Mission Creek strand is thought to have occurred ~500 to 100 ka, as deformation migrated westward onto the Banning and Garnet Hill strands, San Gorgonio Pass fault zone, and northward into the Eastern

[1]Geology Department, San Jose State University, San Jose, CA 95192-0201, USA. [2]U.S. Geological Survey, Earthquake Science Center, Pasadena, CA 91106, USA. [3]Berkeley Geochronology Center, Berkeley, CA 94709, USA. [4]University of California, Berkeley, Berkeley, CA 94720-4767, USA. [5]Western Washington University, Bellingham, WA 98225, USA. [6]U.S. Geological Survey, Earthquake Science Center, Menlo Park, CA 94025, USA.
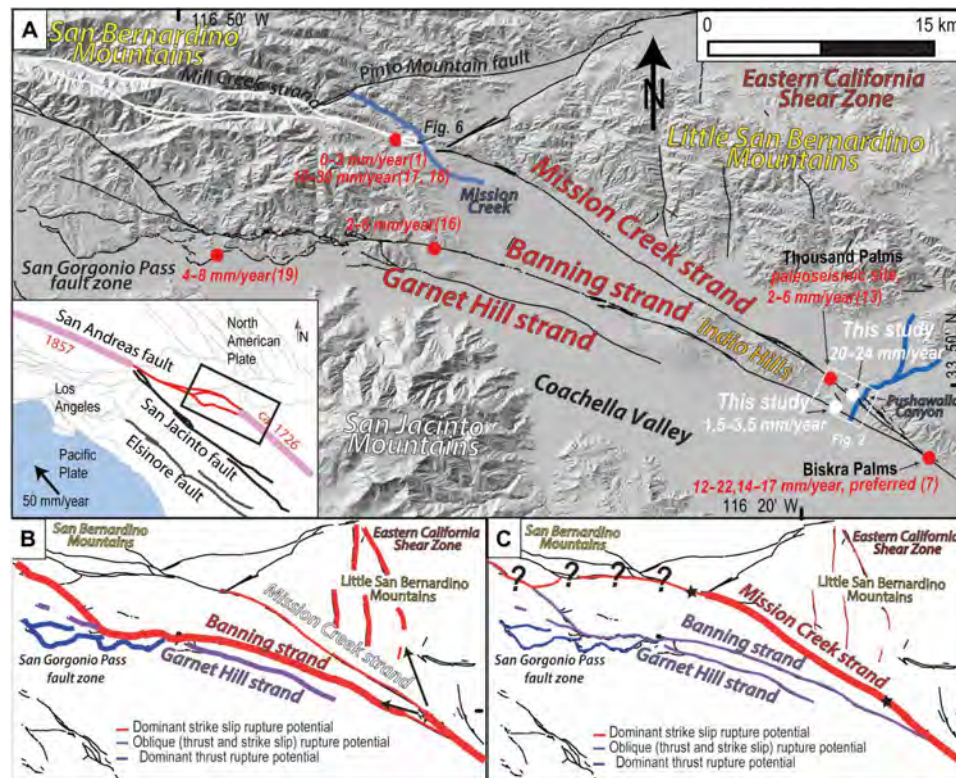*Corresponding author. Email: kimberly.blisniuk@sjsu.edu

Fig. 1. Location map of study area on the southern SAF. (**A**) Map showing the location of the Mission Creek strand, Banning strand, Garnet Hill strand, and San Gorgonio Pass fault zone of the southern SAF. The white circles show the locations of slip rate sites in this study, and red circles show the locations of prior studies. The white rectangles show the locations of Figs. 2 and 6. Black lines show the location of active faults, and white lines show the location of inactive faults proposed in previous studies of the southern SAF (*9–11*). The thick blue lines identify the key drainages discussed in the text and show the source of sediment for channel and terrace deposits from the Little San Bernardino Mountains through Pushawalla Canyon. Topography derived from 10-m NED (National Elevation Dataset) data, U.S. Geological Survey. Inset map shows the southern SAF system, defined by the SAF, San Jacinto fault, and Elsinore fault. Thick pink lines delineate portions of the SAF that last ruptured in 1857 and after 1726 CE (*3*). Black box outlines location of (A). (**B**) Illustration of current kinematic and rupture forecast models that reduce likelihood of Mission Creek strand ruptures and emphasize hazard posed by the strands to the southwest; symbolized here by thickness of lines (black arrows indicating alternative rupture pathways). (**C**) Simplified kinematic and rupture forecast model based on the results from this study, emphasizing constraints from slip rates at either end of the Mission Creek strand (locations shown by black stars). (B) and (C) are modified from (*16*).

California Shear Zone near the Little San Bernardino Mountains (Fig. 1B) [e.g., (*10*, *11*)]. This kinematic model of fault slip distribution suggests that primary plate boundary faults may evolve fairly rapidly by transferring strain across wide zones onto new or reactivated faults. It also informs official earthquake forecasts and has focused attention on the potential for ruptures through the San Gorgonio Pass. Consequently, estimates of 30-year probabilities of a >M (moment magnitude) 6.7 rupture on the Mission Creek strand are low (1.5%) compared to a westerly route linking the Banning and Garnet Hill strands to the San Gorgonio Pass fault zone (12 to 18%), as illustrated in Fig. 1B (*1*). Accordingly, the inferred higher rupture likelihood along the Banning strand, Garnet Hill strand, and San Gorgonio Pass fault zone is used in regional earthquake response planning as exemplified in the ShakeOut Scenario (*12*).

Here, we challenge the consensus that most of the slip is transferred off of the Mission Creek strand and onto other structures. We investigate the long-term deformation rate of the Mission Creek and Banning strands of the SAF in the Coachella Valley, a section of the SAF that has yet to produce a substantial historical earthquake, but where paleoseismic studies suggest frequent ground-rupturing earthquakes (Fig. 1A) (*13*). We then compare our study with dynamic

rupture models (*14*), paleoseismic data (*13*, *15*), and fault slip studies (*7*, *16–19*) to (i) reevaluate the relative roles of the Mission Creek and Banning strands in accommodating surface deformation across the PA-NA plate boundary and (ii) discuss the impact of slip rates on rupture likelihood forecasts for the region.

Study location and approach

Between the drainages of Thousand Palms and Pushawalla Canyon in the Indio Hills, the Mission Creek and Banning strands (Fig. 1A) are well expressed (*20*) and separated by ~4 km at the surface but likely connect at a depth of between 12 and 15 km (*21*). These strands are identified by vegetation lineaments, shutter ridges, beheaded channels, and offset alluvial fans (Figs. 2 to 4). The Mission Creek strand is exposed within the channel walls of Pushawalla Canyon as two prominent fault splays (Figs. 2 to 4), and the subparallel Banning strand is expressed by an offset alluvial fan along the range front of the Indio Hills (Fig. 5). A previous study of the Mission Creek strand at this location by Keller *et al.* (*20*) identified the fault and an abandoned channel (C3; Fig. 2) originating from Pushawalla Canyon that was subsequently offset by ~1 km. In this study, we identify that two more previously unrecognized beheaded channels also offset from
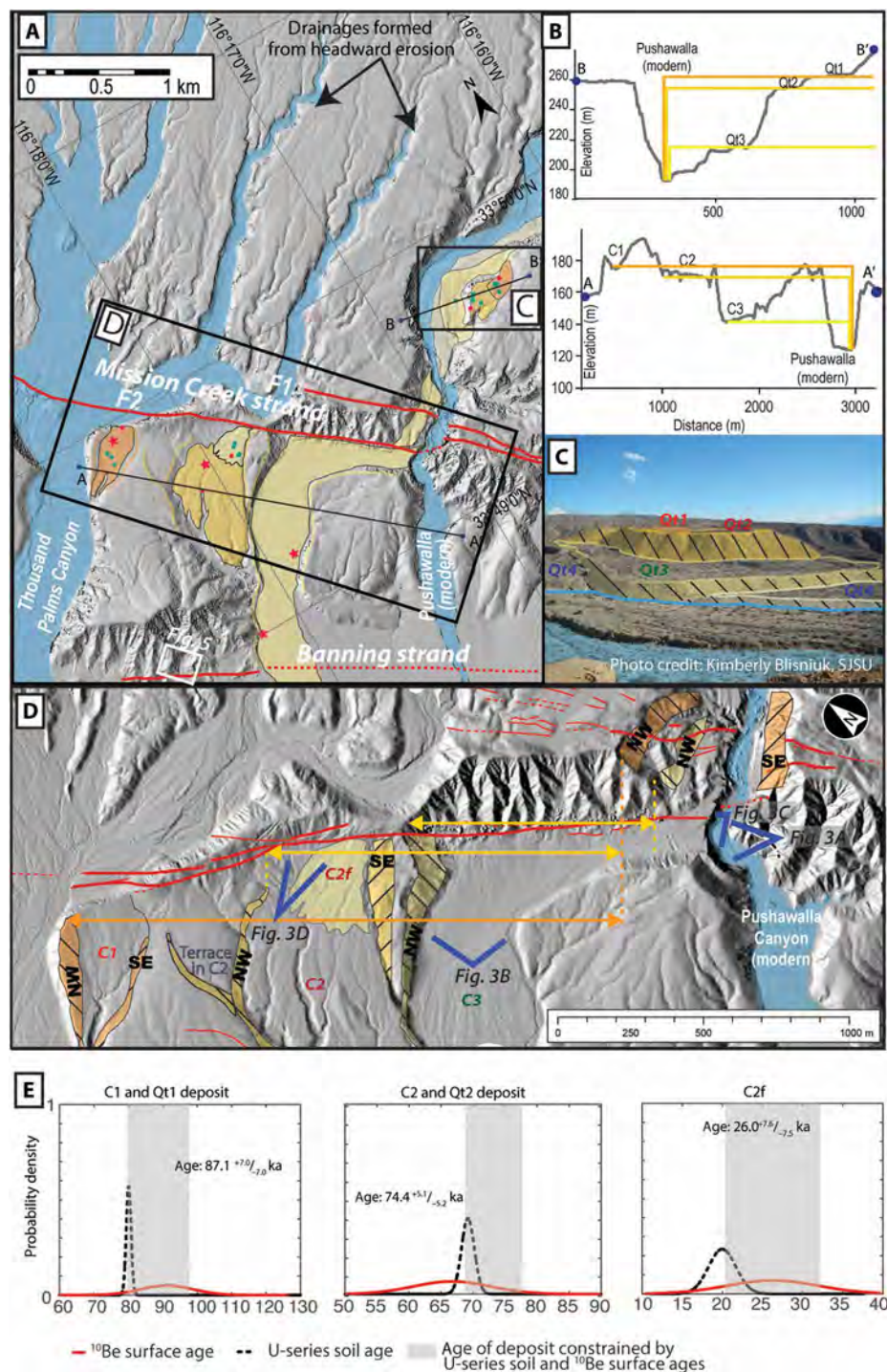
Fig. 2. Summary of offsets and ages along Mission Creek strand at Pushawalla Canyon. (**A**) Hillshade image combines 2-m photogrammetric and 1-m lidar data (*22*). Modern drainages are highlighted in blue, including Pushawalla Canyon, Thousand Palms Canyon (TPC) and two drainages tributary to Thousand Palms Canyon formed by headward erosion. Faults F1 and F2 (red lines) show splays of Mission Creek strand. Locations of dated samples include amalgamated [10]Be surface samples (red stars), [10]Be samples of individual resistant surface clasts (green circles), and U-Th pedogenic carbonate samples from soil pits and excavated channel walls (red circles). Profiles A-A' and B-B' are shown in (B). Black rectangles show locations of (C) and (D) of this figure. White rectangle shows location of Fig. 5. (**B**) Topographic profiles show relief of dated, offset landforms relative to modern Pushawalla Canyon. Note similar relief of terrace treads upstream of fault (B-B') and channel floors downstream of fault (A-A'). (**C**) Photo looking east across Pushawalla Canyon upstream of the fault showing flight of terraces. (**D**) Image showing offsets inferred for channels C1, C2, and C3. Offsets (yellow and orange arrows) are based on restoring channel walls upstream and downstream of the main fault trace (thick red line). Channel walls are highlighted in colored fills and hachuring. SE, southeast walls; NW, northwest walls. Full reconstructions with uncertainties are given in the text and in Fig. 4 and fig. S5. Blue triangles show view direction of photos in Fig. 3. (**E**) Summary of landform ages. Age distributions of [10]Be ages (red) and U-Th ages (black) are modeled using Gaussian probability distributions; gray bars show preferred landform age ranges. See fig. S4 for a plot of all ages. Photo credit: Kimberly Blisniuk, SJSU.

Pushawalla Canyon along the Mission Creek strand (C1 and C2; Fig. 2) and an alluvial fan offset along the Banning strand. We use offsets of these landforms and dates calculated for them using the U-Th soil carbonate and [10]Be surface exposure techniques to calculate slip rates for each fault strand and sum them to obtain the cumulative slip rate across the SAF.

Because of a lack of age control and refined piercing points, a slip rate for the Mission Creek strand was not estimated at Pushawalla Canyon by Keller *et al.* (*20*). However, these authors did estimate a slip rate of 23 to 35 mm/year for the SAF where it is single stranded at the Biskra Palms site, ~5-km southeast of Pushawalla Canyon (Fig. 1). More recent studies that applied multiple numerical dating techniques to the Biskra Palms fan site revised the slip rate there to 12 to 22 mm/year, with preferred rates of 14 to 17 mm/year (Fig. 1) (*7*). The only published slip rate for the Mission Creek strand near Pushawalla Canyon was developed at Thousand Palms Canyon. There, a slip rate of 2 to 6 mm/year since 1000 CE was estimated on the basis of a channel offset of 2.0 ± 0.5 m (*13*).

RESULTS

Mission Creek strand at Pushawalla Canyon

Two fault splays of the Mission Creek strand form a left step at Pushawalla Canyon that produces local folding, uplift, and an angular unconformity between older, mid-Quaternary Ocotillo Formation and younger, overlying cobble-rich fluvial gravels (Fig. 2) (*20*). This deformation appears to have constrained the path of the stream forming Pushawalla Canyon upstream of the fault. The northern fault splay (F1) becomes inactive and is absent at the surface ~1-km northwest of Pushawalla Canyon, and deformation is transferred to the southern fault splay (F2), where the Mission Creek strand is clearly delineated and continues along the northern side of the Indio Hills (Figs. 2A and 3).

Pushawalla Canyon carves a single path through older sediment of the Ocotillo Formation, delivering younger granitoid-rich cobbly sediment from the Little San Bernardino Mountains across the Mission Creek strand via an ephemeral stream (Fig. 1A). The canyon is ~500-m-wide upstream of the fault and abruptly narrows to ~200 m at the fault, which it crosses at a high angle (Fig. 2). Upstream of the Mission Creek strand, a flight of terraces is preserved in the canyon as mantled deposits overlying Ocotillo Formation (*20*), where we mapped four main surfaces (Qt1, Qt2, Qt3, and Qt4) in the field and from lidar data (*22*). The deposits that make up the terraces are distinctly different from those of the Ocotillo Formation. These deposits are 1 to 3 m in thickness, fluvial in nature, and rich in Cretaceous granitoid and gneissic sediment that are derived from the Little San Bernardino Mountains and were likely left behind when the terrace surfaces were abandoned. Downstream of the Mission Creek strand, we identified three beheaded and abandoned paleochannels (C1, C2, and C3) and an alluvial fan (C2f) (Figs. 2 and 3B) that are also incised into the Ocotillo Formation (Fig. 3). Sediment deposits in these paleochannels are also 1 to 3 m in thickness, fluvial in nature, and rich in granitoid and gneissic sediment. Both upstream terrace deposits and downstream deposits
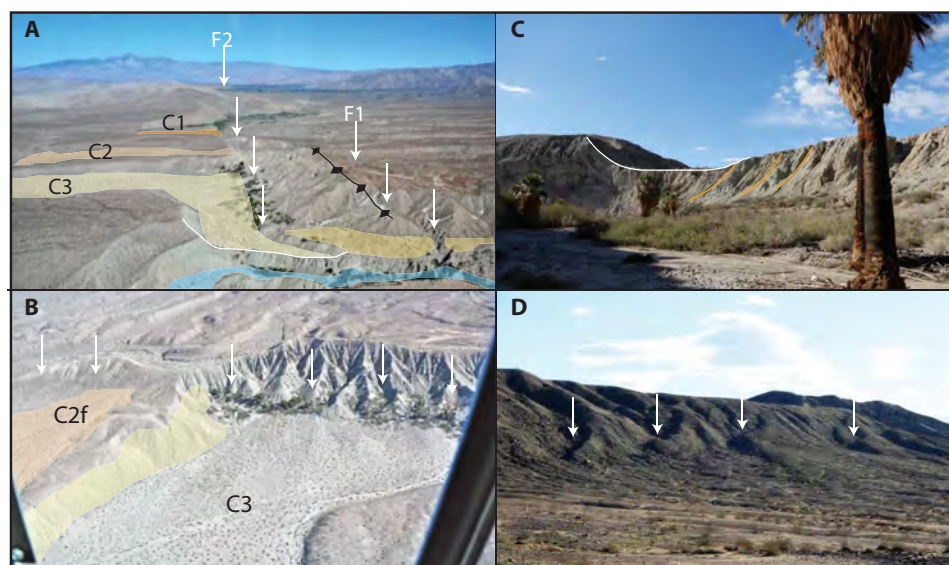

Fig. 3. Photos of Mission Creek strand at Pushawalla Canyon. The white arrows delineate primary geomorphic traces of the fault. Locations shown in Fig. 2. (**A**) Oblique aerial photo looking northwest. The fault here forms a left step, producing a compressional ridge in between the two fault splays, F1 and F2 (*20*). The ridge is shown by the black line with diamonds. The main fault splay, F2, is delineated by a vegetation lineament formed by palm trees and shrubs. Highlighted in blue is present day Pushawalla Canyon. Highlighted in pale yellow, light orange, and dark orange are offset channel deposits, C3, C2, and C1, respectively. The yellow surface is Qt2. All highlighted surfaces are sourced from Pushawalla Canyon. The white line marking the outline of C3 highlights the channel form of C3. Photo credit: Katherine Scharer, USGS. (**B**) Photo taken from above channel C3 looking north showing the geometry of C3 and the Mission Creek strand. The channel wall of C3, highlighted in yellow, is relatively straight and intersects the fault at a high (~90°) angle, indicating that abandonment of C2 and incision of C3 did not occur until this edge was in front of Pushawalla Canyon. Combined with this linear edge, the fault-parallel section of C3 indicates that the channel was first incised across the fault and then deflected before the more recent incision into the modern channel. Highlighted in orange is the fan, C2f, in C2. Photo credit: Katherine Scharer, USGS. (**C**) Photo showing the northwest wall of present day Pushawalla Canyon exposing steeply tilted and folded bedding of the Ocotillo Formation along the fault, indicated by the orange lines. White line is the channel bottom of C3 [see (A)]. (**D**) Photo showing southwest-facing ridge in C2. The white arrows show the location of the fault and shutter ridges produced along it. Photo Credit: Kimberly Blisniuk, SJSU.

in the paleochannels unconformably overlie the Ocotillo Formation and can be observed where more recent erosion has incised into the paleochannels (fig. S2).

We provide multiple lines of geomorphic evidence to support the interpretation that Pushawalla Canyon is the source of incision and subsequent deposition of fluvial deposits into the three paleochannels (C1, C2, and C3). These observations are the following:

1) The topography shows that Pushawalla Canyon is currently the closest through-going stream channel that would have most recently supplied sediment from the Little San Bernardino Mountains, in the form of terrace and fluvial deposits, into those paleochannels (Fig. 2 and fig. S1). The channels are incised into mid-Quaternary Ocotillo Formation, and they are mantled by 1 to 3 m of younger sediment deposited by the stream issuing from Pushawalla Canyon, their only plausible source given their elevations. We note that Fig. 2 and fig. S1 show two other tributary channels on the upstream side of the fault just northwest of Pushawalla Canyon, which were considered as possible sources of channel alluvium across the fault for C2 and C1, respectively. However, we concluded that these were not sources because (i) the tributary channels end in the surface north of the fault and do not connect all the way to the Little San Bernardino Mountains; (ii) the tributary channels do not have evidence for older, higher elevation terrace remnants preserved along them that would be correlative with the elevations of C1 and C2; and (iii) a previous study that examined longitudinal profiles for each of these drainages noted that the tributaries do not show evidence of the uplift associated with the left step between F1 and F2 [20]. We therefore interpret this absence of uplift to indicate that the tributaries are younger than the deformation caused by transfer of slip between F2 and F1 of the Mission Creek strand.

2) The basis of the elevations and morphology of the beheaded channels relative to the tributary channels and the absence of sediment similar to those in C1, the tributary channels cannot be sources of alluvium for the offset paleochannels. We interpret the tributary channels to be formed more recently by processes of headward erosion on the fan surface (Fig. 2 and fig. S1).

3) Folding and tilting of mid-Quaternary Ocotillo Formation on the northeast side of the fault produced the ridge between F1 and F2 that effectively blocks drainage flow from upstream into the three paleochannels (Fig. 2 and fig. S1). This ridge constrains Pushawalla Canyon to a relatively narrow width of 200 m on the northeast side of the fault. Evidence of this constriction is shown by the deflection of the modern drainage near the fault (Fig. 2 and fig. S1).

4) The relief between each terrace riser from Qt1 to Qt2 to Qt3 in Pushawalla Canyon is similar to the progressive decrease in elevation of channel bottoms from C1 to C2 to C3 (Fig. 2B). Specifically, the relief between surfaces C1-C2 and Qt1-Qt2 (~10 m) and the relative elevation of surfaces C2-C3 and Qt2-Qt3 (30 to 35 m) are similar in magnitude (Fig. 2B). This pattern indicates long-term downcutting in response to regional uplift and repeated channel avulsion driven by dextral slip.

Surface characteristics and geochronology of paleochannels and associated terraces

Below, we summarize that field observations and geochronological data indicating that beheaded paleochannels offset by the Mission Creek strand can be correlated with penecontemporaneous terrace surfaces preserved upstream of the Mission Creek strand in Pushawalla Canyon, thereby supporting the fault offsets and landform ages that underlie our new slip rate calculations.

Paleochannel C1 and terrace Qt1. Qt1 is the highest strath terrace within Pushawalla Canyon, preserved at the inside corner of a meander ~1-km upstream from the Mission Creek strand (Fig. 2 and fig. S1). The Qt1 terrace is spatially restricted (150 m by 250 m) and sits ~18 m below a higher Ocotillo Formation pediment. The surface of Qt1 is planar in form, with no bar and swale microtopography evident. Surface clasts are dominated by moderate-sized cobbles. Sparse gneissic and amphibolite cobbles exhibit strong parting along foliations or are disaggregated. Varnish is strong (medium brownish gray), and rubification is strong (dark orange with red-orange rims) on granitic clasts. Many cobbles show rubification on both sides of the clast, indicating that they have been overturned, suggesting reworking and/or inheritance.

We analyzed [10]Be concentrations on the tops of four resistant boulders from Qt1 (PT-1, PT-5, PT-11, and PT-15) and applied U-Th dating to soil carbonate clast coatings from a carbonate-rich horizon 1.3 to 1.0 m below the surface (PT-P1) (fig. S1). The photo of the boulder in fig. S3 from Qt1 provides an example of boulders from which [10]Be surface samples were collected. [10]Be exposure ages range from 89.4 ± 8.5 to 105 ± 8.8 ka (table S1 and fig. S4). Two carbonate clast coatings yielded dates of pedogenesis, and therefore minimum estimates for deposition of host alluvium, of 80.1 ± 0.7 and 65.4 ± 1.5 ka (table S2). The younger U-Th age postdates all [10]Be ages from Qt1 and is younger than U-Th samples collected from soils of C2, so it was not used to bracket the minimum age of deposit Qt1.

C1 is identified as the highest fluvial deposit that is contained within channel wall downstream of the Mission Creek strand (Figs. 2B and 3A). The C1 deposit is located 1900 to 2300 m from its upstream source, Pushawalla Canyon, and is the westernmost of the beheaded channels preserved (Fig. 4 and see the "Offset and slip rate estimates" section under Methods). C1 is 300 m in width at its upstream edge (Fig. 2 and fig. S1), where lateral incision by a tributary of Thousand Palms Canyon has eroded part of the channel near the Mission Creek strand (Fig. 2, A and D). Incision by this tributary exposes bright red soils of the C1 deposit overlying light tan colored Ocotillo Formation (fig. S2F). The surface of C1 is incised by a deep gully near its downstream end, reflecting headward erosion from Thousand Palms Canyon below. Otherwise, the surface of the C1 deposit is relatively planar with no bar and swale microtopography evident (figs. S2E and S3). Surface clasts are dominated by small boulders and cobbles (fig. S3). Amphibolite and gneissic boulders appear strongly varnished (shiny and black) and are commonly split along foliation planes. Weathering characteristics of granitic boulders on the surface are variable; some are deeply grusified, while others preserve a deep strong varnish. Surface clasts exhibit strong rubification with many cobbles showing a deep orange red color on their undersides. Many cobble clasts exhibit rubification on both sides. (fig. S3, C1 surface).

We analyzed [10]Be from five samples taken from C1: three boulder tops (PW-1, PW-3, and PW-4) and two amalgamated samples (PW-5 and PW-6) (fig. S1). The amalgamated samples yielded [10]Be dates of 82.1 ± 6.2 and 90.6 ± 2.0 ka, respectively. While one boulder top (PW-4) yielded a much older age (346.2 ± 30.3 ka), two other boulders yielded ages of 76 ± 6.7 and 94.2 ± 5.9 ka, respectively, which are similar to those of the amalgamated samples (table S1). The photos labeled C1 surface in fig. S3 show the typical clast size sampled from the C1 surface.

Given the similarities in the Qt1 and C1 surfaces and underlying alluvium, including the types and weathering characteristics of
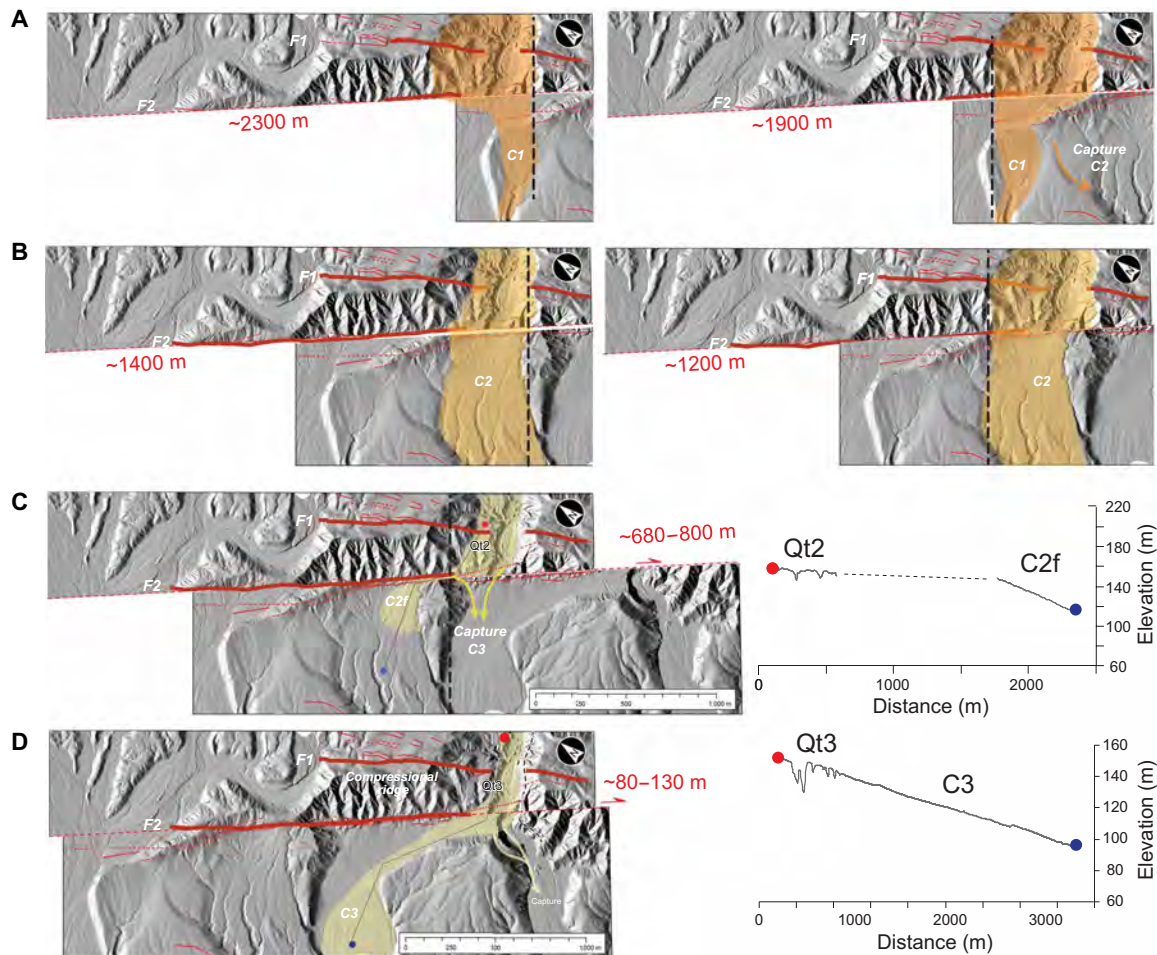
Fig. 4. Digital topography of terrain between Pushawalla and Thousand Palms Canyons along the Mission Creek strand (same area as Fig. 2D) and the reconstruction of preferred offsets of paleochannels C1, C2, C3, and the fan deposit, C2f, in C2 from Pushawalla Canyon. (**A**) Restored view showing preferred offset range needed to realign C1 with Pushawalla Canyon. (**B**) Restored view showing preferred offset range needed to realign C2 with Pushawalla Canyon. (**C**) Reconstruction showing the capture of stream flow by C3 from C2f in C2, with topographic profile showing the gradient of Qt2 and C2f. Red and blue dots show the location of profile across topography connecting Qt2 and C2f (right). (**D**) Reconstruction showing the present capture of stream flow from C3 by modern Pushawalla Canyon, with topographic profile showing the gradient of Qt3 and C3 (right). Limiting minimum and maximum ranges are provided in fig. S5.

surface clasts, microtopography, and their [10]Be and U-Th ages (~80 to 100 ka; fig. S4), we interpret that Qt1 and C1 were incised and abandoned approximately synchronously. We note that [10]Be surface exposure dates of amalgamated pebbles (PW-5 and PW-6) and the tops of individual boulders (samples PW-1, PW-3, PT-1, PT-5, PT-11, and PT-15) are similar, suggesting that the dates are not severely biased by partial shielding, erosion, or inherited [10]Be, since these processes are unlikely to affect the different sample types equally. We calculate an error-weighted mean [10]Be age of 90.4 ± 3.8 ka for Qt1 and C1 from eight similar [10]Be dates (table S1). We interpret boulder PW-4 to be an outlier affected by inheritance because it yielded a [10]Be date of 346.2 ± 30.2 ka; this date is also a statistical outlier. Because we cannot completely rule out inheritance in the [10]Be ages, we adopt a conservative approach to assigning a preferred age to the Qt1 and C1 landforms. That is, we consider the oldest U-series date of 80.1 ± 0.7 ka to provide a minimum age for the Qt1/C1 landform and the upper limit of the mean [10]Be exposure age of 90.4 ± 3.8 ka as the landform's maximum age, yielding an estimated age of 80.1 to 94.1 ka, or 87.1 ± 7.0 ka for the Qt1/C1 landform (Fig. 2E, fig. S4, and tables S1 and S2).

Paleochannel C2 and terrace Qt2. Qt2 is the second highest strath terrace within Pushawalla Canyon upstream of the Mission Creek strand and is inset into the Qt1 terrace (Fig. 2B). The preserved patch of Qt2 is about 200 m by 200 m, and the terrace is ~10 m below Qt1 in elevation (Fig. 2B). The Qt2 surface is planar, with many pebble clasts interlocking and forming a moderate pavement (fig. S3). The surface of Qt2 is dominated by cobbles up to 35 cm in length. Granitic cobbles are moderately varnished (pinkish brown color), while gneissic and amphibolite cobbles exhibit varnish that is medium dark gray in color. A few medium-grained granitic and porphyroblastic gneissic clasts show spallation, producing grus on the surface around the clasts. However, most surface clasts appear smooth and varnished, suggesting little to no weathering of these clasts. Some gneissic and amphibolite clasts show parting along foliations. The underside of many surface cobbles on the Qt2 surface shows moderate orange to pink rubification, and few clasts on the surface exhibit rubification of both sides.

From Qt2, four individual [10]Be surface boulder-top samples were collected (samples PT-16, PT-18, PT-19, and PT-20; table S1 and

fig. S1). The photos labeled Qt2 surface in fig. S3 show the typical boulder sampled from the Qt2 surface. The dates for these samples are 71.2 ± 5.9, 75.8 ± 6.4, 96.9 ± 8.9, and 105.1 ± 8.8 ka (fig. S4). These dates scatter more than expected from their analytical errors, and the two older dates equal or exceed our preferred age for the geologically older C1/Qt1 landform pair, suggesting that the two older samples contain inherited ^{10}Be. U-Th dating of eight carbonate clast coatings from near the basal contact of Qt2 with the underlying Ocotillo Formation (table S2) yielded dates of 7.0 ± 0.8 to 27.6 ± 0.8 ka, younger than the ^{10}Be dates, and too young to represent deposition of Qt2 (table S2).

C2 is the second highest fluvial deposit identified as a paleochannel floor downstream of the Mission Creek strand (Fig. 2). The C2 deposit is located 1200 to 1400 m from the active stream issuing from Pushawalla Canyon and is the second oldest beheaded channel, following C1 (Fig. 4 and see Methods offset reconstruction). The surface of C2 is broad, flat, and ~600 m in width where it terminates against a high ridge along the Mission Creek strand (fig. S2C). Higher terraces are present along the northwest channel wall of C2, preserving an intermediate terrace elevation between C1 and C2 (Fig. 2 and fig. S6). Headward erosion of the C2 deposit has deeply incised the paleochannel floor, locally exposing bright red soils developed in C2 alluvium (fig. S2D). Where not incised by younger erosion, the surface of C2 is fairly smooth, containing poorly sorted subangular pebbles, cobbles, and sparse boulders (fig. S3). Most fine-to-medium–grained granitoid cobbles are grusified in place. Amphibolite and gneissic clasts have rust to almost black varnish developed on their exposed surfaces, with the presence of parting along foliation planes. The undersides of cobble clasts show a range of color intensity from strong to moderate rubification.

From C2, we analyzed one ^{10}Be sample consisting of >100 amalgamated surface clasts (PW-P2-S), which produced an age of 72.6 ± 6.9 ka. No boulders were found that were considered suitable for cosmogenic dating. Four carbonate clast coatings from ~2.2 to 2.4 m in depth yielded mutually consistent U-Th ages with a weighted mean of 69.2 ± 1.4 ka. (table S2 and fig. S4), in good agreement with the ^{10}Be age. On the basis of their similar surface morphology, weathering characteristics, and ^{10}Be and U-series dates, we infer that terrace Qt2 and channel C2 were incised and abandoned synchronously. We consider the mean U-Th age of 69.2 ± 1.4 ka to be a minimum estimate for the Qt2/C2 landform and the mean of three concordant ^{10}Be ages (71.2 ± 5.9, 72.6 ± 6.9, and 75.8 ± 6.4 ka), 72.6 ± 6.9 ka, to provide a maximum estimate for the Qt2/C2 landform. Accordingly, we assign the landform a preferred age range of 69.2 to 79.5 ka or 74.4$^{+5.1}$/$_{-5.2}$ ka. We exclude from consideration ages of two boulders from Qt2 (PT-18 and PT-20) that yielded ^{10}Be dates of 96.9 ± 8.8 and 105.1 ± 8.8 ka, respectively, much older than other ^{10}Be and U-Th dates for C2 and Qt2 but similar to ages calculated for Qt1, suggesting that they were inherited from Qt1.

The northeast corner of C2 contains an alluvial fan, C2f, that abuts the high ridge along the fault and covers part of the interfluve between C2 and C3 (Figs. 2, 3B, and 4). This fan is significant as it is interpreted as the youngest deposit from Pushawalla Canyon in C2. The apex of the fan grades to the elevation of the Qt2 surface, which is located on the northeast side of the fault 680 to 800 m from C2f in Pushawalla Canyon (Fig. 4 and see Methods offset reconstruction). On the basis of the presence of the high-ridge north of the Mission Creek strand, which would block sediment from the tributary canyons (Figs. 2 and 3A), the shape of the fan (bordering the interfluve

and down into the C2 drainage), the elevation of its apex (Fig. 4C), and the similarity of clast size and composition of the fan to that of C1 and C2 deposits, we conclude that Pushawalla Canyon is the source for this fan. In contrast, hillslopes of the high ridge along the Mission Creek strand expose Palm Springs and Ocotillo Formation (Fig. 3C), which consist of mudstones and sandstone, unlike the C2f alluvium that consists of larger cobbles and pebbles of rocks lithologically similar to those of the Little San Bernardino Mountains.

The surface of C2f is undulating and hummocky with preserved but muted bar-and-swale microtopography (fig. S3). Surface clasts are lightly to moderately varnished with bars consisting dominantly of cobble clasts, with some boulders present on the surface. Clast sizes on the surface range from boulders to gravel with 30- to 40-cm-long cobbles as the dominant clast size (fig. S3, C2f surface). Granitic clasts exhibit pinkish-brown varnish, with medium-grained clasts showing evidence of spallation and grusification. Rubification is moderate on well-seated clasts, and some parting is observed in gneissic cobbles.

From C2f, we collected five boulder- and cobble-top samples (PW-9, PW-10, PW-11, PW-13, and PW-14) for ^{10}Be dating and analyzed six pebbles with pedogenic carbonate coatings from the soil at ~1.5 to 1.7 m in depth. The photos labeled C2f surface in fig. S3 show the clast sampled from bars of the C2f surface and a photo of a boulder from C2f. ^{10}Be dates of four of the five samples from the C2f fan surface indicate a mean exposure age of 27.3 ± 6.3 ka. One older ^{10}Be sample (PW-10, 48.4 ± 4.1 ka) is a statistical outlier and likely reflects the presence of inherited ^{10}Be (fig. S4). U-Th dating yielded dates ranging from 11.1 ± 3.0 to 18.9 ± 4.6 ka. The two oldest U-Th ages are concordant with the ^{10}Be dates, and we interpret their mean age of 18.5 ± 4.8 ka as a minimum estimate of the depositional age of the C2f alluvium. Combining this U-series age with the ^{10}Be exposure age for the surface indicates that C2f was abandoned 26.0$^{+7.6}$/$_{-7.5}$ ka (table S1).

Paleochannel C3 and terrace Qt3. The largest preserved patch of Qt3 in Pushawalla Canyon is about 700 m in length by about 100 m in width. Bar and swale microtopography is preserved on the surface, with relative amplitudes (40 cm) similar to the modern wash. The surface is dominated by very coarse gravel to cobble-sized clasts. Cobbles are rounded to subrounded, and felsic-rich clasts are smooth with pale pink to medium pale pink varnish. Rubification on felsic rocks is subtle, dominantly pale orange or pale pink. Scattered about the surface are dark, highly varnished cobbles that are presumed to reflect reworking and inheritance from older deposits. Some bars on the surface include boulders 1 m or more in size. Using ^{10}Be, we dated the tops of two such boulders from Qt3, PT-7 and PT-8, which yielded ages of 31 ± 2.6 and 13.0 ± 1.1 ka, respectively. The date of the older boulder overlaps with the age estimated for C2f (27.3 ± 6.3 ka), and the date of the younger boulder is similar to the date estimated for C3 (fig. S4 and table S1).

C3 is a ~400-m-wide channel deposit lying between steep bedrock side walls that form the paleochannel floor of C3, the most recent beheaded channel from Pushawalla Canyon along the Mission Creek strand (fig. S1) (20). The surface is light gray to pale pink, with muted bar and swale microtopography. The bars are dominated by 20-cm cobbles of subrounded granitoids, amphibolite, and gneiss. Surface clasts are weakly varnished with a pale pink color, and darker clasts appear to be more weathered, or darker on their sides, suggesting that these clasts were likely toppled or had prior exposure. Approximately 10 to 15% of the granitic clasts show surface erosion,

while most are smooth with no apparent weathering observed on their surface. Undersides of granitic clasts are pale orange showing weak to moderate rubification. No parting is observed in more mafic, foliated clasts. Boulders up to 1 m are common in some debris flow bars; some of these boulders have moderate pink varnish that is locally flaking off.

We collected amalgamated samples consisting of >100 pebbles (PW-P7-S and PW-P1-S) from two young debris flow bars that were formed during channel aggradation of C3, one from each side of the channel walls of C3 (Fig. 2A and fig. S1). Sample PW-P7-S (13.7 ± 1.1 ka) was collected from near the west channel wall of C3 to potentially constrain older debris flow deposits, and sample PW-P1-S (11.5 ± 1.1 ka) was collected near the east channel wall of C3 to potentially bracket younger debris flow deposits. [10]Be exposure dating of these two amalgamated samples overlaps within their respective uncertainties, yielding a mean age of 12.7 ± 1.4 ka (table S1 and fig. S4).

Given the similarity in their surface weathering, including weak to moderate varnish development and rubification, lack of parting in amphibolite clasts, and their consistent elevation relative to the gradient of Pushawalla Creek, we infer that Qt3 and C3 were formed and abandoned around the same time. The age of incision postdates the C2f deposit (26.0$^{+7.6}$/$_{-7.5}$ ka), and abandonment is dated by the mean date of two amalgamated samples of cobble bars within C3 (12.7 ± 1.4 ka) and a single boulder date from Qt3 (PT-8, 13 ± 1.3 ka)

Interpretation of paleochannel reconstruction and displacement

We interpret the similarities of the absolute ages, relative elevations, observed surface characteristics of fluvial deposits, and age-related surface properties between the terraces and paleochannel deposits across the fault to indicate synchronous deposition of Qt1 and C1, Qt2 and C2, and Qt3 and C3, respectively (Fig. 2 and fig. S4). These results indicate that C1 and Qt1 were incised and abandoned by 87.1 ± 7.0 ka and C2 and Qt2 were incised and abandoned by 74.4$^{+5.1}$/$_{-5.2}$ ka. Terrace Qt3 in Pushawalla Canyon yielded dates between 13.0 ± 1.0 and 31.0 ± 2.6 ka, which overlap with the dates for both the incision of C3 and abandonment of C2f (fig. S5).

To determine offset along the Mission Creek strand, we summarize the progression of drainage capture and slip along the fault over time based on dates estimated in this study. The best example of progressive drainage capture and downcutting comes from the youngest of the paleochannels (C3) at Pushawalla Canyon (Fig. 4C) (20). We interpret that C3 was cut and then accrued dextral slip, resulting in a large deflection of C3 of at least 680 m (Fig. 4C). This occurred sometime after ~26 ka based on the ages in C2f, C3, and Qt3. Avulsion has produced a weak left jog in the present Pushawalla Canyon. Restoring the modern channel, where Pushawalla Canyon has recently incised ~20 m, to the width of the canyon upstream of the fault permits 80 to 130 m of slip since C3 was abandoned (Fig. 4D).

Before channel avulsion and downcutting to create C3, deposition of a fan in C2, C2f, occurred along the southeast edge of C2 near the fault (Figs. 3B and 4C). The similarity in elevation of the strath of the Qt2 terrace near the fault and the apex of the C2f surface provides strong evidence that C2f graded to Qt2 (Fig. 4C and fig. S1). Deposition of a fan across and then along the fault (Fig. 4C) may reflect the reduced slope produced as C2 was translated away from the canyon mouth, or a climatic period of reduced transport. Accordingly, the last time that alluvium was deposited in C2 from Pushawalla Canyon should be closely constrained by the age of the C2f fan surface. Reconstruction of the incised western channel wall

of C3 suggests that at least 680 m (and as much as ~800 m) of dextral slip has accumulated since abandonment of the C2f fan. This range in displacement values reflects possible reconstructions that allow drainage connectivity between Qt2 (i.e., the width of the upstream channel during Qt2 time) and the C2f surface. The slip rate calculated from this offset uses the abandonment age of the C2f surface (i.e., 26.0$^{+7.6}$/$_{-7.5}$ ka) and the offset range of 680 to 800 m (table S4).

Incision and deposition of the C2 surface into the Ocotillo Formation resulted in a prominent, arcuate fluvial scarp bounding the northwestern channel margin of C2 (fig. S5). Realignment of this scarp with the back edge of the Qt1 terrace across the fault suggests a maximum offset of 1800 m since original cutting of C2 (fig. S5A). A similar value of 1800 m of slip realigns the southeast channel wall of Pushawalla Canyon to the west channel wall of C2 (fig. S5B). A minimum offset for C2 of 1050 m is determined by aligning the back edge of the Qt2 terrace with the west edge of the alluvial fan deposit, C2f (fig. S5C). The preferred offset reconstruction of 1200 to 1400 m simply aligns the channel walls of Pushawalla Canyon with the preserved channel walls of paleochannel C2 north and south of the fault, respectively (Fig. 4B). The preferred slip rate is calculated using this offset value, 1200 to 1400 m, and the dates from C2 and Qt2 of 74.4$^{+5.1}$/$_{-5.2}$ ka (Fig. 2E and fig. S4).

C1 is smaller and has a narrower width than the other paleochannels (Fig. 2). The edge of C1 closest to the fault has been eroded back about 150 m from the fault by tributaries of Thousand Palms Canyon. Evidence of alluvial deposition from Pushawalla Canyon into C1 is preserved where we observed (i) a reddish younger soil on top of older mid-Quaternary light colored alluvium (fig. S2F), (ii) the form of C1, which has gently sloped channel walls that grade toward the flat channel bottom (fig. S1B), (iii) intermediate small terrace remnants that are inset into the channel walls within C1 (fig. S3), and (iv) the presence and age of a Qt1 terrace located on the upstream side of the fault that provides evidence that flow from Pushawalla Canyon likely shaped the topographic form of C1. Reconstruction of the gently sloped northwest channel wall of C1 with the 500-m-wide mouth of Pushawalla Canyon suggests between 1900 and 2300 m of slip occurred since original cutting of C1 (Fig. 4A). The preferred slip rate calculated for C1 uses this offset value of 1900 to 2300 m and the age of 87.1 ± 7.0 ka for the C1 surface (Fig. 4 and table S4). We also calculate a minimum slip rate for C1 using the maximum offset of C2 (1700 to 1800 m); the uncertainty is determined by realigning the terrace riser of C2 across the fault, which we interpret to represent the initial incision of C2 (fig. S5 and table S4). The minimum slip rate for C1 combines this 1700- to 1800-m offset of C2 with the age of the C1 surface (fig. S6B and table S4).

We calculated preferred and minimum slip rates for the Mission Creek strand over three time intervals, since 87.1 ± 7.0, 74.4$^{+5.1}$/$_{-5.2}$, and 26.0$^{+7.6}$/$_{-7.5}$ ka (fig. S6) based on ages of offset paleochannels and an offset alluvial fan. Projection and realignment of the channel walls of C1, C2, and C3 yield preferred offsets of 2300 to 1900 m and 1400 to 1200 m for C1 and C2, respectively (Fig. 4). The offset of each reconstruction is the midpoint value between the range of displacements, and the uncertainty of each offset is the distance from this midpoint to the maximum and minimum displacements (table S4). The calculated average slip rate applies a linear fit to the offsets and ages of all offset channels, using code provided in (23) and using uniform probability distributions based on maximum and minimum values for age and offset distance, and calculates the probability distribution of the fault's slip rate using Monte Carlo sampling. The

linear average preferred slip rate on the Mission Creek strand for these three time intervals since ~95,000 years is 21.6 ± 2 mm/year (2σ) (fig. S6A). A limiting minimum slip rate of 20.7 ± 2 mm/year (2σ) is also calculated by combining the age of C1 with the maximum offset of C2 and by combining the age of the alluvial fan, C2f, with the maximum offset of C3 (fig. S6B and table S4). Slip rates of 20.7 ± 2 mm/year (2σ) provide a minimum rate for the Mission Creek strand during this time interval because aggradation of the channel floor in C1 and the C2f fan in C2 must predate or be synchronous with the incision of the west channel walls of C2 and C3, respectively (Fig. 4 and fig. S5). This minimum rate is similar to calculated estimates of 20.7 ± 3.6 mm/year, when applying ^{10}Be surface dates of the oldest clasts from each offset landform and the limiting maximum and limiting minimum offset values, demonstrating that slip rates appear to be relatively insensitive to the details of the age interpretations.

To encompass all rates for the Mission Creek strand consistent with our data, we also calculate limiting maximum and limiting minimum rates based on dextral offsets of 2500 to 1800 m, 1800 to 1050 m, and 800 to 680 m for C1, C2, and C3, respectively, which yields estimated slip rates of 22.6 ± 4 mm/year (2σ). See offset reconstruction shown in fig. S5.

Banning strand, Indio Hills
Just south of the Mission Creek strand at Pushawalla Canyon, three closely spaced traces of the Banning strand were identified and mapped at the Washington Street site (24). These splays vertically and horizontally offset an alluvial fan along the Indio Hills (Fig. 5). The alluvial fan, Qf3b, is sourced locally from a small catchment that delivers reworked mid-Quaternary sediment and alluvium from the Ocotillo and Palm Springs Formations (Fig. 5). The surface of the Qf3b fan is light tan in color and is hummocky with preserved but muted bar-and-swale microtopography (Fig. 5E). Cobble to gravel clasts are scattered on the surface, with 15- to 20-cm-long cobbles as the dominant clast size within bars. These clasts appear fresh, angular to subangular, and unvarnished to lightly varnished, indicating a Holocene age deposit.

The subsurface alluvium of the fan is characterized by a silty matrix with many interbedded pebble lenses. We collected six gravel samples for a ^{10}Be depth profile model age, including one from the surface on a bar and five samples from the subsurface (table S2). ^{10}Be concentrations of profile samples decrease exponentially with depth, yielding a model age of $6.1^{+2.2}/_{-2.0}$ ka for the fan surface (Fig. 5A and table S3). One sample, BF-P1-b, was not used in the model age calculation because the uncertainty of the measured ^{10}Be concentration of this sample was significantly larger (~2×) than the remaining five samples. We also applied U-Th dating to nine samples of soil carbonate clast coatings collected at two different depth intervals, from 100 to 120 cm and 160 to 190 cm (table S2). The mean of the four oldest reproducible clast-coat ages is 139.9 ± 8.1 ka. Unlike samples from the Pushawalla slip rate site on the Mission Creek strand, where U-series dates either overlapped or were younger than the ^{10}Be exposure dates, U-series dates of 139.9 ± 8.1 ka from the Qf3b deposit are significantly older than the $6.1^{+2.2}/_{-2.0}$ ka ^{10}Be
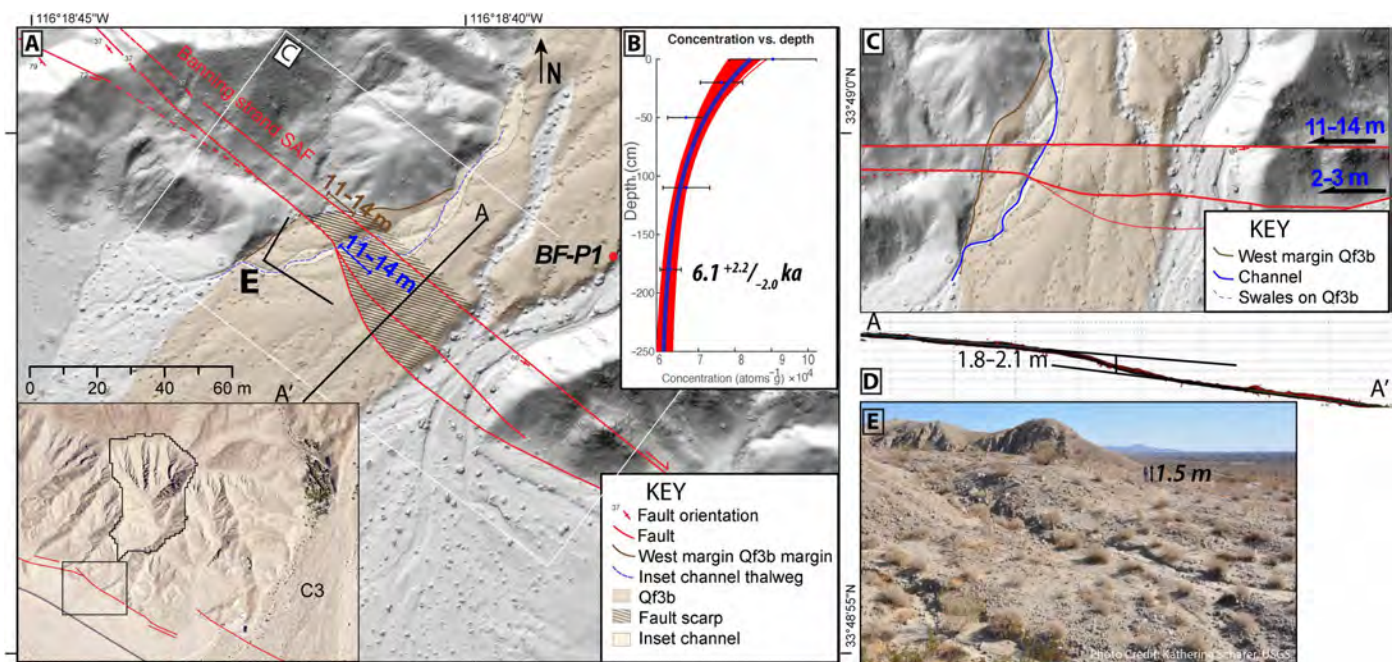

Fig. 5. Summary of Banning strand, Washington Street site in the Indio Hills showing offset landforms and ages. (**A**) Composite hillshade image on the Banning strand showing a mapped Qf3b alluvial fan offset along three splays of the fault. The red circle shows the location of the ^{10}Be depth profile and U-series samples collected from the surface and subsurface. Blue and brown offsets of 11 to 14 m are based on reconstruction of northwestern fan margin and a channel thalweg shown in (B). Image produced from data in (24) and (22). Inset map is aerial image showing the location of this site near southern end of paleochannel C3. Black line demarks drainage area of Qf3b. See Fig. 2A for location. (**B**) Modeled ^{10}Be depth profile (and associated age range) showing a decrease in ^{10}Be concentration with depth following procedures summarized in (34). (**C**) Reconstruction of the offset alluvial fan, aligning the edge of the fan and an incised channel thalweg (indicated by brown and blue lines, respectively). (**D**) Topographic profile A-A′ across the Qf3b fan in (A) showing vertical displacement of the fan. (**E**) Field photo of the fault scarp offsetting the Qf3b alluvial fan, with person for scale. Location shown in (A). Photo credit: Katherine Scharer, USGS.

depth profile model age. On the basis of overall surface morphology, the relatively young appearance of the Qf3b surface, and the position of the Qf3b fan in the landscape, we interpret the $6.1^{+2.2}/_{-2.0}$ ka to best represent the age of the deposit. We interpret our results to indicate that the sampled carbonate was derived primarily from clasts reworked from older deposits, given the small catchment size and proximal source of the alluvial fan.

Observed faulting of the Qf3b alluvial fan is distributed over an ~20-m-wide zone that includes two distinct southwest-facing scarps, offsets of bars and swales, and offset of an incised channel (Fig. 5A). The northeastern-most fault splay exhibits the largest horizontal displacement of the Qf3b fan surface. A maximum horizontal offset of 14 m is measured across this splay by realigning the west edge of the Qf3b fan where it is in contact with Ocotillo Formation bedrock (brown lines in Fig. 5, A and C). A minimum offset of 11 m on the northern splay realigns the thalweg of a deflected channel that is incised into the Qf3b fan (Fig. 5C). A second, central splay of the Banning strand right-laterally offsets swales and an intervening bar by 2 to 3 m (Fig. 5, A and C). The third (southwestern) splay of the Banning strand does not exhibit measurable lateral displacement of the Qf3b surface. A topographic profile measured across all three splays indicates 1.8 to 2.1 m of vertical displacement (Fig. 5D). Combining the ^{10}Be depth profile model age of $6.1^{+2.2}/_{-2.0}$ ka with the cumulative horizontal offset of 13 to 17 m and vertical displacement of 1.8 to 2.1 m yields a Holocene lateral slip rate of 2.5 ± 1 mm/year (2σ) mm/year and vertical slip rate of $0.3^{+0.2}/_{-0.1}$ mm/year for the Banning strand at the Washington Street site.

DISCUSSION

Our new slip rate for the SAF in the Indio Hills is 24.1 ± 3 mm/year (2σ), obtained by summing rates across the Mission Creek (21.6 ± 2 mm/year) and Banning strands (2.5 ± 1 mm/year). This is similar to rates on the SAF ~125 km to the northwest at Cajon Pass (25) and to the high end of rates of 12 to 22 mm/year reported a few km to the south at Biskra Palms, although we note that the preferred rate of 14 to 17 mm/year at Biskra Palms is somewhat lower (Fig. 1) (7). A slip rate of 24.1 ± 3 mm/year is also similar to present-day geodetic slip rates at this latitude (4) estimated across the entire southern SAF. Our calculated slip rate represents about half of the deformation across the PA-NA plate boundary.

These results support a model in which the Mission Creek strand is the primary plate boundary fault at the latitude of our study, 33° 50′, and show that SAF surface ruptures from past and potentially future earthquakes are likely to be larger and more frequent on the Mission Creek strand in the northern Coachella Valley than currently inferred in earthquake forecasts (1). This emerging picture stands in contrast to previous interpretations of the SAF at this latitude.

Previous kinematic models for this region of the SAF inferred that slip rates decrease along the Mission Creek strand to a few millimeters per year northwest of Biskra Palms as the SAF bifurcates and begins to form a restraining bend near the Little San Bernardino Mountains (7–11) and, furthermore, that slip along the Mission Creek strand is transferred to the west onto the Banning strand, Garnet Hill strand, and San Gorgonio Pass fault zone and to the north onto the Eastern California Shear Zone (Fig. 1B). The inference of a marked decrease in Mission Creek strand slip was apparently supported by a slip rate of 2 to 6 mm/year proposed at Thousand Palms (13) and a rate of 0 to 3 mm/year estimated for the continuation of the strand to the

northwest (1) and has been attributed to the geometric complexity of the SAF in the San Gorgonio Pass region (9–10). The Banning strand, Garnet Hill strand, and San Gorgonio Pass fault zone are therefore predicted by existing models to take up most of the lateral displacement and seismic hazard potential at this latitude. In particular, the combined Banning and Garnet Hill strands through Coachella Valley are considered to have the highest slip rate (4 to 16 mm/year) among the SAF strands in this region in recent earthquake forecasts (1).

Here, we question those models and contend that the majority of slip on the Mission Creek strand does not transfer westward onto the Banning strand and that the Mission Creek strand may remain active along its restraining bend near the San Bernardino Mountains. Below, we develop several considerations relevant to this possibility.

Our preferred (21.6 ± 2 mm/year) and minimum (20.7 ± 2 mm/year) slip rate estimates for the Mission Creek strand are notably faster than a slip rate of 2 to 6 mm/year just north of Pushawalla Canyon at Thousand Palms Canyon calculated in an earlier study (Fig. 1) (13). However, we note that the slip rate of 2 to 6 mm/year at Thousand Palms is the result of displacement from only two to three earthquakes on fault strands exposed in trenches and may not include other deformation across a broader aperture on the strand given the discontinuous nature of surface faulting expressed in the trenches (13). Accordingly, we conclude that this earlier study does not provide a robust long-term average for all slip on the Mission Creek strand.

On the Banning strand, our new Holocene slip rate of 2.5 ± 1 mm/year is within the range of a Holocene slip rate of 2 to 6 mm/year estimated at a location ~30 km to the northwest along this fault, as it enters the San Gorgonio Pass (Fig. 1) (16). Given the overlap in these two rates for the Banning strand, it is possible that the Holocene slip rate remains constant along the fault between the two sites, although an increase in as much as a factor of two along the 30-km length of the fault strand cannot be ruled out with the present data. However, our new Banning strand slip rate of 2.5 ± 1 mm/year at Indio Hills and rates of 2 to 6 mm/year (16) near the San Bernardino Mountains account for only a small fraction ($\sim^1/_5$) of total SAF slip as the fault enters the San Gorgonio Pass. These relatively slow Holocene slip rates along the Banning strand do not support a model where the majority of plate boundary motion is accommodated by this structure.

In contrast, an active Mission Creek strand from the Indio Hills to the San Bernardino Mountains is consistent with more frequent ground-rupturing earthquakes observed at the Thousand Palms paleoseismic site (average repeat time, ~215 years) than on the Banning strand or San Gorgonio Pass fault zone (average repeat times, ≥500 years) (13, 15). This idea is supported by several other studies, including dynamic rupture models that show ruptures readily transfer from the Coachella section to the Mission Creek strand, but not the Banning strand (14); geodetic studies that include an active Mission Creek strand (4); and recent geologic studies that suggest mid to late Pleistocene slip rates of 10 to 30 mm/year on the Mission Creek strand near its restraining bend in the San Bernardino Mountains (Fig. 1A), based on 2.4 to 2.5 km of displacement since ~260 to 100 ka (17, 18).

Previous studies (8, 10–11, 26) note observations of the subdued tectonic expression of offset landforms in Holocene to late Pleistocene deposits northwest of the Indio Hills to infer inactivity of the Mission Creek strand. To address the apparent paradox between previous studies and more recent data, we highlight evidence of recent active

faulting along the Mission Creek strand based on our observations and consultant paleoseismic trenches (27). Just west of Mission Creek, we find ~50-m offsets of ephemeral drainages incised into late Pleistocene surfaces (17) and offsets of gullies in steep-walled canyons, which we infer to likely be Holocene in age (Fig. 6). Although these offsets are not yet dated, their presence on the Mission Creek strand provides evidence of more recent faulting at this latitude than previously thought. We suggest that the range in offset amounts observed and apparent ages based on regional geochronology of alluvial fan surfaces (26) to indicate that the Mission Creek strand is active as it enters the San Bernardino Mountains along the restraining bend of the SAF. Last, trenching investigations along the Mission Creek strand just east of Mission Creek show faulting in alluvium on some of the mapped strands, although clear expression of the faults is not present on the surface (27). We speculate that scarps along the Mission Creek strand are less apparent in the topography because the Mission Creek strand is closer to the range front, where streams more readily bury and erode scarps, while vertical separation across the Banning strand enhances its appearance at its more distal position.

The combination of a high slip rate on the Mission Creek strand in the Coachella Valley from the Indio Hills to possibly the southern San Bernardino Mountains and evidence of late Quaternary activity

Fig. 6. Evidence of late Quaternary offsets on the Mission Creek strand west of Mission Creek (see Fig. 1A for location). (A) Shaded topography of area from lidar (22). Red line shows fault trace offsetting features; gray dashed line bounds northern edge of fault zone based on a damage zone mapped in the field. Four catchments (black lines) and thalwegs (light blue) incised into late Pleistocene (26) surface deposits are highlighted. **(B)** Field photograph looking northwest along recent trace. View location shown in (C). Oblique view to southwest highlights right lateral offsets of steep Holocene gullies that establish recent fault motion on the Mission Creek strand (red arrows). **(C)** Backslipping catchments by 50 to 60 m restores geometry of catchments and channel thalwegs across the Mission Creek strand (red). Note that in Fig. 1A, the Mission Creek strand has been considered inactive at this location west of Mission Creek. Black arrow marks northern extent of damage zone; note crushed rocks in lower right. Beheaded and deflected drainages and consistent right-lateral displacement in this area indicate tectonic motion. **(D)** Image is composite of lidar from (22) and photogrammetric model provided by K. Johnson outlined in white, scale variable but shows ~0.5 km of the fault. Processing as in (24). Photo credit: Katherine Scharer, USGS.

in the area of Mission Creek (Fig. 6) may shed light on the three-dimensional geometry of the SAF, where the complex tectonic history led to the appellation of the "San Gorgonio Knot" (9–10). Many workers have tried to unravel the knot with geologic (9, 10) and geophysical investigations (28), and interpretations of the structure have varied over time (6). A major challenge in deciphering the subsurface geometry of the SAF near the San Gorgonio Pass is the paucity of seismicity along the major fault strands. Neither the Mission Creek nor Banning strands are illuminated by microseismicity in the upper crust, although a ~5-km step in the base of seismicity below the surface trace of the Mission Creek strand (29) suggests a subvertical discontinuity there. Recent seismicity in the northern Coachella Valley, such as the moderate 1986 North Palm Springs event (moment magnitude, 6.0) and its aftershocks, is generally interpreted as the down-dip expression of the Banning or Mission Creek strands (29). Alternatively, other studies have emphasized a major north-dipping structure tied to the Banning strand and San Gorgonio Pass fault zone and dismissed activity on an upper crustal extension of a steeply dipping Mission Creek strand (30). A recent study of seismic wave speeds along the Mission Creek strand supports continuity of fault structure through this region but proposes that ruptures would not traverse the full length of the strand (31). In combination, a fast-slipping Mission Creek strand in the Indio Hills, evidence of late Quaternary to recent offsets at Mission Creek (Fig. 6) (17, 18), and recent seismic reflection studies (21) indicate that the geometry of the SAF at seismogenic depths is likely a hybrid of a steeply dipping, through-going Mission Creek strand and north-dipping faults associated with the Banning and Garnet Hill strands and the San Gorgonio Pass fault zone. We do not propose that the Banning strand, Garnet Hill strand, or the San Gorgonio Pass fault strands are inactive; rather, we suggest that up to half of the strain from PA-NA horizontal plate motion is accommodated by slip along the Mission Creek strand in the northern Coachella Valley. If so, then our new results and interpretations suggest that continental transform plate boundaries, such as the mature SAF, may remain relatively stable over tens of thousands of years and plate boundary deformation may migrate more slowly than suggested by existing evolution models (10).

It remains unclear where slip is transferred from the Mission Creek strand to the northwest into the San Bernardino Mountains. We speculate that some slip may continue along the Mission Creek and Mill Creek strands or other, unidentified fault strands to the west, and then link to the San Bernardino strand and some may be transferred onto the Eastern California Shear Zone through motion on the Pinto Mountain fault (11). More work is needed to constrain fault slip rates in this region and to examine the accommodation by broadly distributed or plastic deformation and uplift within the San Bernardino Mountains (32). While our study results may not affect existing models of shaking for the Los Angeles region modeled for ruptures along the Banning strand and San Gorgonio Pass fault zone [e.g., (33)], we are not aware of studies that examine the effects of rupture directivity along a more northerly route. An increased slip rate for the Mission Creek strand will likely affect fault displacement hazard estimates for major infrastructure in the area (6, 12). We suggest that the Mission Creek strand may have a higher rupture likelihood than is currently estimated (1) and that a future SAF earthquake could link the Mission Creek strand with other faults in the San Bernardino Mountains (Fig. 1). Given the elapsed time since the ca. 1726 CE earthquake (3) and the high slip rates found in
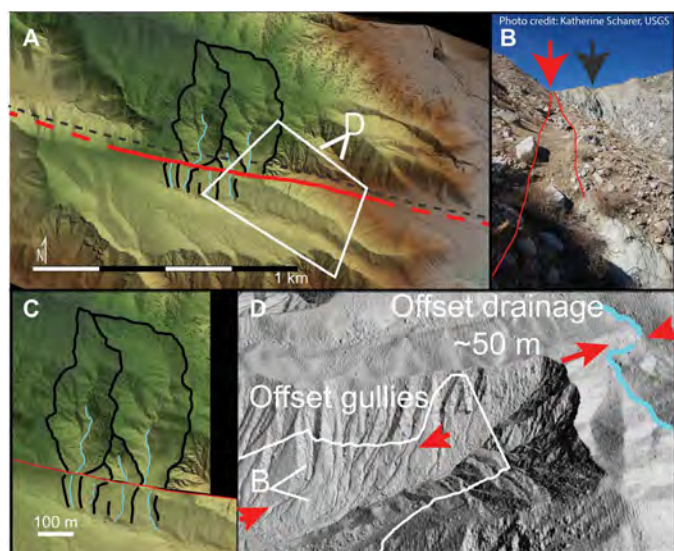
this study, 6 to 9 m of elastic strain may have accumulated on the Mission Creek strand. The Mission Creek strand transects major water and power infrastructure that serves the greater Los Angeles region but has received less attention than other faults such as the Banning strand, Garnet Hill strand, and San Gorgonio Pass fault zone in regard to earthquake effects.

METHODS
We completed field mapping of the Mission Creek and Banning strands and the Indio Hills on hillshade maps derived from lidar data (*22*) at 1:1000 scale to identify the best slip rate site for the region. Field mapping revealed multiple locations for slip rate studies. Pushawalla Canyon was selected as the main site for detailed mapping and geochronologic studies because it preserves multiple landforms offset across the fault at a single location and dateable features on both sides of the Mission Creek and Banning strands of the SAF.

Channel and terrace deposits, C1, C2, C2f, C3, Qt1, Qt2, and Qt3, were differentiated in the field based on overall geomorphologic character and the degree of weathering exhibited by surface clasts to establish relative ages of deposits. Observations made of each surface included the degree of desert pavement development, the preservation of bar-and-swale morphology, relative smoothness and texture of surface clasts, and the degree of channel dissection. Observations made of surface clasts for each deposit included the degree of grusification and fracturing, the degree of desert varnish development, and the degree of rubification on the undersides of surface clasts. Numerical ages of paleochannels, alluvial fans, and terraces were estimated by dating the uppermost alluvium preserved on each landform via ^{10}Be surface exposure dating and U-Th dating of pedogenic carbonate clast coatings.

^{10}Be surface exposure dating
Three sampling protocols were used to obtain material for ^{10}Be dating (table S1). Boulders and large cobbles were sampled by collecting chips from the top 2 cm of the largest clasts available from each surface. These samples were collected from clasts exhibiting smooth surfaces, minimal postdeposition eolian erosion, and minimal grusification. Sampled boulders were embedded into their respective surfaces, suggesting that they had remained stable since deposition. A second sampling technique involved amalgamating many pebbles and small cobbles (8 to >100 clasts) from the surface of the deposit into a single sample, thereby providing an average ^{10}Be exposure date for the landform. The third sampling technique involved collecting sand and gravel samples from the surface and subsurface for a cosmogenic depth profile. Rock types of sampled clasts include quartz-rich rocks, including quartzites, gneisses, and granitoids, such as tonalities and quartz monozonites, originating from the Little San Bernardino Mountains. All chemical and analytical processing for cosmogenic exposure ages followed the procedures described in (*34*). The ^{10}Be depth profile model age was calculated following procedures and a MATLAB code summarized in (*35*). All ^{10}Be surface exposure ages were calculated using the CRONUS Age Calculator version 3 (*36*). Ages are reported at the 2σ level.

Except for a single depth profile age, ^{10}Be dates in this study are not corrected for inheritance. This correction, which typically consists of subtracting the ^{10}Be present in samples taken from an active wash from dating samples, was not applied in this study because a previous study in the region found that these corrections for ^{10}Be

inheritance yielded anomalously young exposure ages of landforms, probably because the landscape is not in steady state (*34*).

U-Th dating
Field and laboratory sampling protocols for U-Th dating of pedogenic carbonate were similar to those of (*37*). For "no-chem." samples (see table S2), solutions were aliquoted to yield fractions containing 0.1 to 0.2 mg of carbonate and analyzed via inductively coupled plasma mass spectrometer (ICP-MS). For most samples, U and Th were separated from matrix elements using anion exchange chemistry, reacted with HNO_3 and $HClO_4$ to remove residual organic material, and analyzed via ICP-MS. Samples were analyzed using both conventional and no-chem. procedures and yielded ages in good agreement (table S2).

Carbonates were analyzed using a Thermo Fisher Scientific Neptune Plus ICP-MS in solution mode using analytical protocols described in (*38*). Activity ratios and ages were calculated using the half-lives of (*39*) for ^{238}U, (*40*) for ^{232}Th, and (*41*) for ^{230}Th and ^{234}U. Correction for U and Th from detritus was made assuming activity ratios of (^{232}Th/^{238}U) = 1.2 ± 0.5, (^{230}Th/^{238}U) = 1.0 ± 0.1, and (^{234}U/^{238}U) = 1.0 ± 0.1. Ages and uncertainties were calculated with Isoplot 3.75 (*42*). Uncertainties of corrected ages are reported at the 2σ level and include measurement errors, procedural ^{230}Th blanks, and uncertainties associated with detritus corrections but not decay constants (*43*). U-Th data and ages are reported in table S2.

Estimating final landform ages
If postdepositional erosion has not significantly modified a geomorphic surface, then ^{10}Be exposure dates should yield the maximum age of the surface when no correction is made for inheritance, as for the Mission Creek strand samples in this study. U-series dating of pedogenic carbonate, in contrast, provides minimum estimates of depositional age since pedogenic carbonate forms after deposition of host alluvium. Accordingly, where both ^{10}Be and U-Th ages are available (i.e., channel-terrace pairs C1/Qt1 and C2/Qt2, and fan C2f), we estimated ages of landforms as follows. We interpret their mean ^{10}Be exposure age (excluding outliers) as a maximum age estimate and the oldest U-Th age or ages as a minimum age estimate. Where multiple mutually consistent U-Th ages defined the oldest U-Th age (i.e., C2), we used their weighted mean age as the minimum landform age. For the remaining landforms where no U-Th ages were available, ages were inferred from bracketing ^{10}Be ages (C3/Qt3) or from a ^{10}B depth profile (Qf3). Note that detailed interpretations of the ^{10}Be and U-Th ages of each landform are given on a case-by-case basis in the "Surface characteristics and geochronology of paleochannels and associated terraces" section.

Offset and slip rate estimates
To estimate the amount of displacement on the Mission Creek strand at Pushawalla Canyon, we realigned offset features based on image reconstruction and geomorphic interpretation of progressive channel avulsion driven by dextral slip (Fig. 4 and fig. S5). Eroded remnants of Ocotillo Formation on the southwest side of the fault appear to periodically block upstream drainage and flow from Pushawalla Canyon (Fig. 4). Figure 4 shows our preferred interpretation of the long-term downcutting in response to this uplift and the avulsion of channels C1, C2, and C3 and present day Pushawalla Canyon. Figure S5 shows the maximum and minimum interpretation of the long-term downcutting in response to this uplift and the avulsion of channels C1, C2, and C3 and present day Pushawalla Canyon.

To determine the magnitude of displacement for each beheaded paleochannel, the preserved northwestern and southeastern channel walls of C1, C2, and C3 were projected to the Mission Creek strand and aligned to Pushawalla Canyon along the fault on a composite 1-m lidar basemap in ArcMap (Fig. 4). Paleochannel walls of C1, C2, and C3 are defined by their relief and geomorphology and correlated with terrace risers within Pushawalla Canyon upstream of the fault (Figs. 1A and 2, B and D). Preferred maximum displacement values for C1 and C2 are estimated by aligning the present southeast channel wall of Pushawalla Canyon upstream of the fault with the southeast channel walls of C1 and C2 (Fig. 4). Preferred minimum displacement values for C1 and C2 align the high terrace risers along the northwest wall of Pushawalla Canyon upstream of the fault with the northwest channel walls of C1 and C2 (Figs. 2 and 4). We also estimate limiting maximum and limiting minimum offset measurements for the incision of beheaded channels C1 and C2. The limiting maximum offset measurement values align the northwest channel wall downstream of the fault to the preserved southeast channel wall of modern Pushawalla Canyon (fig. S5). The limiting minimum offset measurement for beheaded channel C1 aligns the highest terrace riser (representing capture of C2) in C2 downstream of the fault to Pushawalla Canyon upstream of the fault (fig. S5). The minimum offset measurement for beheaded channel C2 is determined by aligning the alluvial fan C2f in C2 downstream of the fault to its preserved terrace floor upstream of the fault (fig. S5).

SUPPLEMENTARY MATERIALS

Supplementary material for this article is available at http://advances.sciencemag.org/cgi/content/full/7/13/eaaz5691/DC1

REFERENCES AND NOTES

1. E. H. Field, G. P. Biasi, P. Bird, T. E. Dawson, K. R. Felzer, D. D. Jackson, K. M. Johnson, T. H. Jordan, C. Madden, A. J. Michael, K. R. Milner, M. T. Page, T. Parsons, P. M. Powers, B. E. Shaw, W. R. Thatcher, R. J. Weldon II, Y. Zeng, Long-term time-dependent probabilities for the third Uniform California Earthquake Rupture Forecast (UCERF3). *Bull. Seismol. Soc. of Am.* **105**, 511–543 (2015).
2. M. Gerstenberger, B. Fry, Preface to the focus section on the joint Japan–Taiwan–New Zealand National Seismic Hazard Model Collaboration. *Seismol. Res. Lett.* **87**, 1236–1239 (2016).
3. T. K. Rockwell, A. J. Meltzner, E. C. Haaker, Dates of the two most recent surface ruptures on the southernmost San Andreas fault recalculated by precise dating of Lake Cahuilla Dry Periods. *Bull. Seismol. Soc. Am.* **108**, 2634–2649 (2018).
4. K. A. Guns, R. A. Bennett, J. C. Spinler, S. F. McGill, New geodetic constraints on southern San Andreas fault-slip rates, San Gorgonio Pass, California. *Geosphere* **17**, 39–68 (2020).
5. J. Beyer, M. L. Cooke, S. T. Marshall, Sensitivity of deformation to activity along the Mill Creek and Mission Creek strands of the southern San Andreas fault. *Geosphere* **14**, 2296–2310 (2018).
6. R. Weldon, G. de Lamare, D. Yule, W. Hammond, A. Streig, A. Sarmiento, S. Freeman, J. Shamma, M. Beikae, A. Rodriguez, San Andreas fault – South Branch surface deformation modeling and risk to the Colorado River Aqueduct, in *Applied Geology in California*, R. Anderson, H. Ferriz, Eds. (Association of Environmental and Engineering Geologists, 2016), pp. 147–219.
7. W. M. Behr, D. H. Rood, K. E. Fletcher, N. Guzman, R. Finkel, T. C. Hanks, K. W. Hudnut, K. J. Kendrick, J. P. Platt, W. D. Sharp, R. J. Weldon, J. D. Yule, Uncertainties in slip-rate estimates for the Mission Creek strand of the southern San Andreas fault at Biskra Palms Oasis, southern California. *Geol. Soc. Amer. Bull.* **122**, 1360–1377 (2010).
8. C. R. Allen, San Andreas fault zone in San Gorgonio Pass, southern California. *Geol. Soc. Amer. Bull.* **68**, 315–350 (1957).
9. D. Yule, K. Sieh, Complexities of the San Andreas fault near San Gorgonio Pass: Implications for large earthquakes. *J. Geophys. Res.* **108**, 2548 (2003).
10. J. C. Matti, D. M. Morton, Paleogeographic evolution of the San Andreas fault in southern California: A reconstruction based on a new cross-fault correlation, in *The San Andreas Fault System: Displacement, Palinspastic Reconstruction, and Geologic Evolution*, R. E. Powell, R. E. Weldon II, J. C. Matti, Eds. (Geological Society of America, 1993), **178**, pp. 107–159.
11. K. J. Kendrick, J. C. Matti, S. A. Mahan, Late quaternary slip history of the Mill Creek strand of the San Andreas fault in San Gorgonio Pass, southern California: The role of a subsidiary left-lateral fault in strand switching. *Geol. Soc. Am. Bull.* **127**, 825–849 (2015).
12. L. M. Jones, R. L. Bernknopf, D. A. Cox, J. Goltz, K. W. Hudnut, D. S. Mileti, S. Perry, D. J. Ponti, K. A. Porter, M. S. Reichle, H. A. Seligson, K. Shoaf, J. Treiman, A. M. Wein, "The ShakeOut Scenario: Effects of a potential M7. 8 earthquake on the San Andreas fault in southern California" (USGS Open-File Report 2008-1150, California Geological Survey, 2008).
13. T. E. Fumal, M. J. Rymer, G. G. Seitz, Timing of large earthquakes since AD 800 on the Mission Creek strand of the San Andreas fault zone at Thousand Palms Oasis, near Palm Springs, California. *Bull. Seismol. Soc. Am.* **92**, 2841–2860 (2002).
14. R. Douilly, D. D. Oglesby, M. L. Cooke, J. L. Hatch, Dynamic models of earthquake rupture along branch faults of the eastern San Gorgonio Pass region in California using complex fault structure. *Geosphere* **16**, 474–489 (2020).
15. K. M. Scharer, D. Yule, A maximum rupture model for the Southern San Andreas and San Jacinto faults, California, derived from paleoseismic earthquake ages: Observations and limitations. *Geophys. Res. Lett.* **47**, e2020GL088532 (2020).
16. P. Gold, W. M. Behr, D. Rood, W. D. Sharp, T. Rockwell, K. J. Kendrick, A. Salin, Holocene Geologic slip rate on the Banning strand of the southern San Andreas fault, southern California. *J. Geophys. Res.* **120**, 5639–5663 (2015).
17. J. C. Fosdick, K. Blisniuk, Sedimentary signals of recent faulting along an old strand of the San Andreas fault, USA. *Sci. Rep.* **8**, 12132 (2018).
18. G. Balco, K. Blisniuk, A. Hidy, Chlorine-36/beryllium-10 burial dating of alluvial fan sediments associated with the Mission Creek strand of the San Andreas fault system, California, USA. *Geochronology* **1**, 10.5194/gchron-2019-2, (2019).
19. R. Heermance, D. Yule, Holocene slip rates along the San Andreas fault system in the San Gorgonio Pass and implications for large earthquakes in southern California. *J. Geophys. Res.* **44**, 5391–5400 (2017).
20. E. A. Keller, M. S. Bonkowski, R. J. Korsch, R. J. Shlemon, Tectonic geomorphology of the San Andreas fault zone in the southern Indio Hills, Coachella valley, California. *Geol. Soc. Am. Bull.* **93**, 46–56 (1982).
21. R. D. Catchings, M. J. Rymer, M. R. Goldman, G. Gandhok, San Andreas fault geometry at desert hot springs, California, and its effects on earthquake hazards and groundwater. *Bull. Seismol. Soc. Am.* **99**, 2190–2207 (2009).
22. M. Bevis, K. Hudnut, R. Sanchez, C. Toth, D. Grejner-Brzezinska, E. Kendrick, D. Caccamise, D. Raleigh, H. Zhou, S. Shan, W. Shindle, A. Yong, J. Harvey, A. Borsa, F. Ayoub, R. Shrestha, B. Carter, M. Sartori, D. Phillips, F. Coloma, "The B4 project: Scanning the San Andreas and San Jacinto fault zones" (Fall Meeting: abstract #H34B-01, American Geophysical Union, 2005).
23. R. Styron, Slip Rate Calculator, v. 0.1.2. Zenodo (2015); http://dx.doi.org/10.5281/zenodo.33360.
24. K. Johnson, E. Nissen, S. Saripalli, J. R. Arrowsmith, P. McGarey, K. Scharer, P. Williams, K. Blisniuk, Rapid mapping of ultrafine fault zone topography with structure from motion. *Geosphere* **10**, 969–986 (2014).
25. R. Weldon II, K. Sieh, Holocene rate of slip and tentative recurrence interval for large earthquakes on the San Andreas fault, Cajon Pass, southern California. *Geol. Soc. Am. Bull.* **96**, 793–812 (1985).
26. L. A. Owen, S. J. Clemmens, R. C. Finkel, H. Gray, Late Quaternary alluvial fans at the eastern end of the San Bernardino Mountains, southern California. *Quat. Sci. Rev.* **87**, 114–134 (2014).
27. Leighton and Assoc. Geologic Fault and Seismic Investigation, Mission Creek Fault, T2S, R3E, Riverside County, California, Project 6790444-05, 106 p, 2 plates (1981).
28. V. E. Langenheim, R. C. Jachens, J. C. Matti, E. Hauksson, D. M. Morton, A. Christensen, Geophysical evidence for wedging in the San Gorgonio Pass structural knot, southern San Andreas fault zone, southern California. *Geol. Soc. Am. Bull.* **117**, 1554–1572 (2005).
29. C. Nicholson, Seismic behavior of the southern San Andreas fault zone in the northern Coachella valley, California: Comparison of the 1948 and 1986 earthquake sequences. *Bull. Seismol. Soc. Am.* **86**, 1331–1349 (1996).
30. S. Carena, J. Suppe, H. Kao, Lack of continuity of the San Andreas fault in southern California: Three-dimensional fault models and earthquake scenarios. *J. Geophys. Res.* **109**, B04313 (2004).
31. P.-E. Share, Y. Ben-Zion, Bimaterial interfaces in the south San Andreas fault with opposite velocity contrasts NW and SE from San Gorgonio Pass. *Geophys. Res. Lett.* **43**, 10,680–10,687 (2016).
32. M. L. Cooke, L. C. Dair, Simulating the recent evolution of the southern big bend of the San Andreas fault, Southern California. *J. Geophys. Res.* **116**, B04405 (2011).
33. K. B. Olsen, S. M. Day, J. B. Minster, Y. Cui, A. Chourasia, M. Faerman, R. Moore, P. Maechling, T. Jordan, Strong shaking in Los Angeles expected from southern San Andreas earthquake. *Geophys. Res. Lett.* **33**, L07305 (2006).
34. K. Blisniuk, M. Oskin, K. Fletcher, T. Rockwell, W. Sharp, Assessing the reliability of U-series and ^{10}Be dating techniques on alluvial fans in the Anza Borrego Desert, California. *Quat. Geochron.* **13**, 26–41 (2012).
35. A. J. Hidy, J. C. Gosse, J. L. Pederson, J. P. Mattern, R. C. Finkel, A constrained Monte Carlo approach to modeling exposure ages of cosmogenic nuclides: An example from the Lees Ferry, Arizona. *Geochem. Geophys. Geosyst.* **11**, Q0AA10 (2010).
36. G. Balco, J. O. Stone, N. A. Lifton, T. J. Dunai, A complete and easily accessible means of calculating surface exposure ages or erosion rates from ^{10}Be and ^{26}Al measurements. *J. Quat. Geochronol.* **3**, 174–195 (2008).

37. K. E. K. Fletcher, W. D. Sharp, K. J. Kendrick, W. M. Behr, K. W. Hudnut, T. C. Hanks, ^{230}Th/U dating of a late Pleistocene alluvial fan along the southern San Andreas fault. *Geol. Soc. Am. Bull.* **122**, 1347–1359 (2010).

38. W. D. Sharp, C. A. Tryon, E. M. Niespolo, N. D. Fylstra, A. Tripathy-Lang, J. T. Faith, ^{230}Th/U burial dating of ostrich eggshell. *Quat. Sci. Rev.* **219**, 263–276 (2019).

39. J. L. Bischoff, R. W. Williams, R. J. Rosenbauer, A. Aramburu, J. L. Arsuaga, N. Garcíía, G. Cuenca-Bescós, High-resolution U-series dates from the Sima de los Huesos hominids yields $600^{+\infty}_{-66}$ kyrs: Implications for the evolution of the early Neanderthal lineage. *J. Archaeol. Sci.* **34**, 763–770 (2007).

40. J. L. Arsuaga, N. Garcíía, G. Cuenca-Bescós, Precise measurement of half-lives and specific activities of ^{235}U and ^{238}U. *Phys. Rev.* **C4**, 1889–1906 (1971).

41. N. E. Holden, Total and spontaneous fission half-lives for uranium, plutonium, americium and curium nuclides. *Pure Appl. Chem.* **61**, 1483–1504 (1989).

42. H. Cheng, R. Lawrence Edwards, C.-C. Shen, V. J. Polyak, Y. Asmerom, J. Woodhead, J. Hellstrom, Y. Wang, X. Kong, C. Spötl, X. Wang, E. Calvin Alexander Jr., Improvements in ^{230}Th dating, ^{230}Th and ^{234}U half-life values, and U–Th isotopic measurements by multi-collector inductively coupled plasma mass spectrometry. *Ear. & Plan. Sci. Lett.* **371-372**, 82–91 (2013).

43. K. R. Ludwig, Using Isoplot/Ex, version 3.75: A geochronological toolkit for Microsoft Excel, *Berkeley Geochronology Center Special Publication 1a* (Berkeley Geochronology Center, 2010), p. 47.

Acknowledgments

Science Advances

A revised position for the primary strand of the Pleistocene-Holocene San Andreas fault in southern California

Kimberly Blisniuk, Katherine Scharer, Warren D. Sharp, Roland Burgmann, Colin Amos and Michael Rymer